Ultrasonics 54 (2014) 997–1004

Contents lists available at ScienceDirect

Ultrasonics

journal homepage: www.elsevier.com/locate/ultras

Shear horizontal (SH) ultrasound wave propagation around smooth corners

P.A. Petcher *, S.E. Burrows, S. Dixon **

Department of Physics, University of Warwick, Coventry CV4 7AL, UK

ARTICLE INFO

Article history:
Received 3 October 2013
Received in revised form 15 November 2013
Accepted 25 November 2013
Available online 1 December 2013

Keywords:
Shear horizontal (SH) waves
Propagation
Reflection
PPM EMAT
Ultrasonics

ABSTRACT

Shear horizontal (SH) ultrasound guided waves are being used in an increasing number of non-destructive testing (NDT) applications. One advantage SH waves have over some wave types, is their ability to propagate around curved surfaces with little energy loss; to understand the geometries around which they could propagate, the wave reflection must be quantified. A 0.83 mm thick aluminium sheet was placed in a bending machine, and a shallow bend was introduced. Periodically-poled magnet (PPM) electromagnetic acoustic transducers (EMATs), for emission and reception of SH waves, were placed on the same side of the bend, so that reflected waves were received. Additional bending of the sheet demonstrated a clear relationship between bend angles and the reflected signal. Models suggest that the reflection is a linear superposition of the reflections from each bend segment, such that sharp turns lead to a larger peak-to-peak amplitude, in part due to increased phase coherence.

1. Introduction

Shear horizontal (SH) ultrasound waves are polarised in-plane, with respect to a reference interface (typically a sample surface), and are a form of guided wave, although they can be treated as bulk waves under certain conditions, such as over short propagation distances. There are multiple symmetric and anti-symmetric SH wave modes; the phase and group speeds are dependent on frequency, sample thickness, and the bulk shear wave speed [1,2]. This work uses only the lowest order SH mode, SH0 (and generation frequencies are chosen to predominantly generate this mode), which is a symmetric dispersionless mode, and has a speed equal to the bulk shear wave speed in the medium.

SH guided wave ultrasound has been found to travel around tightly curved sections of a propagation medium with only negligible reflection, allowing for inspections to be undertaken, despite such bends between the emitting and receiving EMATs and the section being tested. This work models and experimentally measures the reflection of an SH guided wave upon encountering a curved section of a sample, and has implications not only for inspections on otherwise flat samples, but also for inspections on vessels and pipes, particularly at bends in pipes and at the ends of vessels.

2. Shear horizontal ultrasound in non-destructive testing

SH waves have several properties that are of benefit to non-destructive testing (NDT). For example, a shear wave with polarisation parallel to a boundary is reflected without mode conversion (independent of the incident angle), and the amplitude does not change (there is a π phase shift) [1,3,4]. If SH waves are polarised parallel to the direction of an austenitic weld, they will propagate through with less reflection, beam steering, and attenuation, in comparison to (for example) shear vertical (SV) and compression waves, and they will not mode-convert upon interaction with a defect in the weld that extends parallel to the welding direction [5,6]. This leads to an increase in sensitivity to defects, and hence SH waves are ideal for the development of ultrasonic inspection systems for welds [5–10]. More complicated than inspecting austenitic welds, is the inspection of dissimilar metal welds, not only due to the anisotropic grain structure, but also due to the change in acoustic impedance between the two metals, and SH waves have also been used successfully for that purpose [7].

Thickness steps are often encountered in NDT inspections. Welds (such as a butt joint) can have a thickness step, which make the use of the dispersionless lowest SH mode (SH0) favourable, as it can transfer between the plates without significant reflection at the step [9]. However, different mode conversion behaviour, and changes in the reflection and transmission of the waves, is observed depending on whether the thickness change is gradual

** Co-corresponding author. Tel.: +44 2476573877; fax: +44 2476573133.
E-mail addresses: P.A.Petcher@warwick.ac.uk (P.A. Petcher), S.E.Burrows@warwick.ac.uk (S.E. Burrows), S.M.Dixon@warwick.ac.uk (S. Dixon).

0041-624X
http://dx.doi.org/10.1016/j.ultras.2013.11.011

or sudden, and the extent of the thickness change. For example, SH0 will convert into SH1, if a region of more than twice the thickness is suddenly encountered by the wave, and this process is reversed for a thickness change the other way (SH1 to SH0). However, there is no conversion (and less reflection) for a smooth transition to a different thickness for SH0, and SH1 will reflect completely at the cut-off thickness, rather than mode convert [11]. In addition, SH guided waves have been used to accurately measure sample thickness to better than 1% accuracy for sheets of at least 1.5 mm thickness, without any calibration for material properties [12].

Guided waves can be used for defect detection in pipes, and SH vibration in the circumferential direction can be used to receive torsional and flexural ultrasound wave modes in a pipe [13,14]. Pipe inspection can be performed using SH waves without using them to form a specific pipe wave mode, and this has been demonstrated at inspection distances of up to 20 m [10].

2.1. Shear horizontal ultrasound propagation in curved sections

SH guided wave propagation (including the dispersion curves), is most simple to solve for an isotropic plate (with a constant thickness), of infinite extent in the direction of the wave oscillation. Such a solution is commonly presented in the literature, including the important results of a non-dispersive SH0 mode and cut-off frequency-thickness values for the other modes [1,2]. When travelling around a corner, the waves can still be considered as SH guided waves, since the oscillation is still perpendicular to the propagation direction (Fig. 1 is an example of SH guided wave propagation around a corner), but they are not identical to SH guided waves in a flat plate. There are solutions for SH guided wave propagation under other conditions, and an important one in this case is for SH guided waves propagating circumferentially in a linearly elastic isotropic hollow cylinder. The relevance to this work is that a plate with a curve that has a constant radius of curvature and thickness, with the oscillation perpendicular to the curvature and the plate of large extent in that direction, could be approximated as an isotropic hollow cylinder over the curved region.

Some important results for SH guided waves propagating circumferentially in a linearly elastic isotropic hollow cylinder, that differ from the flat plate case, are that the lowest order mode is no longer non-dispersive, nor is it the fastest mode in energy propagation at high frequencies, and each higher-order mode has a maximum group speed at a finite frequency-thickness [15]. The phase speed curves are qualitatively very similar between the two cases, and for both, as the frequency-thickness tends to infinity, the phase and group speeds of all the modes approach the shear wave speed. If the thickness is kept constant, but the radius of curvature increased (so that the inner radius and outer radius become increasingly similar), the propagation characteristics become more similar to the flat plate case of the same frequency-thickness, until they are identical for the infinite radius of curvature case [15].

Of course, a bend in a flat plate is not identical to a linearly elastic isotropic hollow cylinder. In addition to the presence of the change between the flat plate case and the constant radius of curvature case, there are experimental differences. For example, the plate was originally flat; cold working used to introduce the curve will change the dislocation structure and the microstructure more generally, and hence introduce a change in the material properties between the curved and flat sections of the plate; a change in the wall thickness of that region could also be expected. In addition, unlike with an isotropic cylinder, a constant radius of curvature cannot be guaranteed for a plate that has been cold worked using a manually operated bending machine, and when taking the measurements, the shear wave emitted and received may not propagate exactly circumferentially around the curve. Despite these concerns, it is still possible to consider the waves within the curved region as SH guided waves, albeit with different properties from those in the flat section of the plate.

3. Shear horizontal ultrasound emission and reception

SH waves are usually generated using electromagnetic acoustic transducers (EMATs), for which the mode of operation is extensively documented in the literature [16–23]. Advantages include avoiding the use of couplant, and operating on curved surfaces without being profile matched (although matching them can improve signal levels). The design of SH wave EMATs varies, but for this work, SH guided waves were emitted and received effectively using a periodic-permanent-magnet (PPM) EMAT [24–26], as depicted in Fig. 2. The EMATs have a series of permanent magnets providing a static magnetic field, arranged such that the north and south (N/S) poles alternate periodically. A coil of wire runs parallel to the direction of the periodicity of the magnets, which will create eddy currents in the sample, that lead to a Lorentz force parallel to the surface and perpendicular to the direction of the wire [24,27]. Ideally, this should only generate SH guided waves in a plate [24], although deviations from the ideal case, at the edges of the EMAT, mean that other wave modes (such as Rayleigh–Lamb wave modes) are also generated. Due to the closely spaced elements of the magnet array used in the construction of these

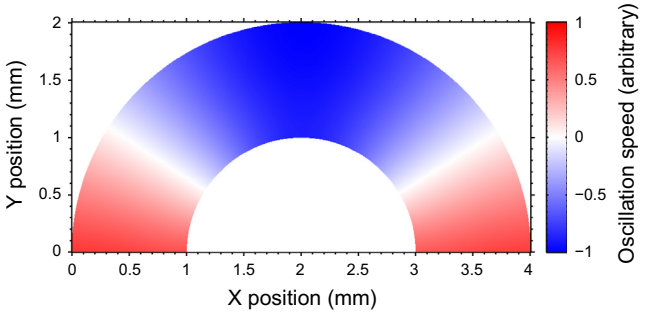

Fig. 1. Finite element method simulation of an SH0 wave propagating around a 1.5 mm radius of curvature corner, in a 1 mm thick piece of aluminium. The amplitude decrease from the outer surface to the inner surface is less than 12% in this case.

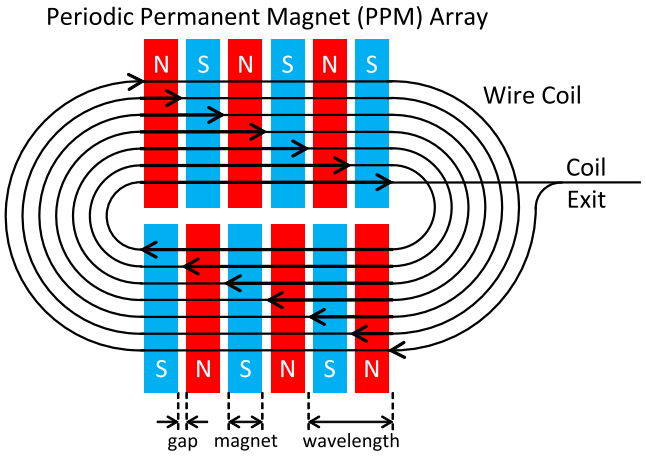

Fig. 2. A PPM EMAT for emission and reception of SH waves. The rows of 2.5 mm width magnets are arranged with 0.5 mm gaps between them, such that the magnetic field switches direction (from up to down) every 3 mm; this provides a 6 mm wavelength. The "racetrack" coil is made using 0.2 mm diameter wire (including insulation).

EMATs, they need to be relatively close to the surface of the sample, to ensure that the forces generated in the sample surface have a strong, periodic variation, that mirrors the periodic variation of the transducer array. An SH guided wave is emitted in the direction of the periodic variation, with a fundamental wavelength that is equal to the spatial repetition of the N/S magnet pairs.

PPM EMATs are used experimentally to conduct this study, and have been approximated in simulations as a series of impulses with alternating polarisations in the direction parallel to the sample surface and perpendicular to the direction of propagation. In both cases, SH guided waves are efficiently emitted using this method. Experimentally, the SH guided waves are received using a PPM EMAT, whereas within simulations, a point-receiver is used.

4. Simulating shear horizontal wave propagation on curved sections

Simulations using the finite element method (FEM) software PZFlex, allow the reflection from curved sections of a sample to be investigated under ideal conditions. The simulation was carried out in two dimensions, with the third dimension the only one in which the SH guided wave can oscillate. The simulated measurement of the waveform will not be dependent on distance from the curved sections, since a guided wave cannot spread out geometrically in two dimensions, and the simulated sample has no damping.

The sample was simulated as being an isotropic, homogeneous, aluminium plate of uniform 1 mm thickness, with a shear wave speed of 3111 m/s. The aluminium plate is modelled as two straight sections, joined by a curved section that has a precisely defined radius of curvature. A series of curves were constructed, with angles ranging from 0° (a completely straight section) to 180° (the second section is parallel to the first), and radiuses of curvature from 0.5 mm to 3 mm. An example 135° curve is shown in Fig. 3. Note that the angle of curvature is measured as the deviation from the flat plate case, and represents the angle the plate has been bent by, rather than the internal angle of the curve. A brief discussion of how the model was created is required to demonstrate how it will relate to a physical experiment.

The centre of the first straight section extends from $(x_0, 0)$ to (x_0, y_0), where y_0 is the length of the straight section, 90 mm for these models. The section has a thickness, $2x_0$, which in this case is 1 mm (as can be seen in Fig. 3b), so that for a given y value along the line, it extends from $(0, y)$ to $(2x_0, y)$. Next, there is a curved section with radius of curvature r, following the path from (x_0, y_0) to (x_1, y_1):

$$x_1 = x_0 + r(1 - \cos\theta) \tag{1}$$

$$y_1 = y_0 + r\sin\theta \tag{2}$$

The angle varies in the range $0 \leqslant \theta \leqslant \theta_{max}$, where θ_{max} is the final curve angle, making the curve a section of a circle. The arc has the same thickness as the straight section, meaning that the inner curve has a radius of curvature of $r - x_0$ and the outer curve has a radius of curvature of $r + x_0$. The second straight section, of length l, extends from (x_1, y_1) to (x_2, y_2):

$$x_2 = x_1 + l/\sqrt{1 + \cot^2\theta} \tag{3}$$

$$y_2 = y_1 + (\cos\theta/|\cos\theta|)l/\sqrt{1 + \tan^2\theta} \tag{4}$$

As with the other segments, this line has a thickness of $2x_0$ (1 mm), with a length of 60 mm.

In order to measure the reflection, the emitter and receiver were located on the same side of the curve, considering the reflected signal rather than changes to the transmitted signal. The emitter, modelled as a 6 mm wavelength PPM EMAT, with 3 pairs of oppositely polarised magnets, is centred at $(2x_0, y_0R)$ (on the inner part of the curved surface), where $R = 3/4$. Elements in one direction are placed at $(2x_0, y_0R - 6)$ to $(2x_0, y_0R - 3)$, $(2x_0, y_0R)$ to $(2x_0, y_0R + 3)$, and $(2x_0, y_0R + 6)$ to $(2x_0, y_0R + 9)$, and in the other direction are placed at $(2x_0, y_0R - 9)$ to $(2x_0, y_0R - 6)$, $(2x_0, y_0R - 3)$ to $(2x_0, y_0R)$, and $(2x_0, y_0R + 3)$ to $(2x_0, y_0R + 6)$, with units of millimetres. For the surface region over which they extend, the emitter elements apply a tangential impulse to the simulation nodes at the very surface of the sample. The form of this impulse is that of four cycles of a 518.5 kHz wave, with the force inverted for the opposite element directions. The receiver is placed at $(2x_0, y_0R + 9)$, which is just after the end of the emitter.

The space between nodes in the square mesh used was 10 μm, such that at the dominant wavelength of 6 mm, there are 600 nodes per wavelength. It was confirmed that the simulations had converged by comparing the results to those obtained in a simulation with elements of double the size (20 μm, half the resolution). The difference between the outputs was very small, certainly negligible relative to the absolute magnitude of the reflected wave. There is an issue with the implementation of these models, with regard to small radiuses of curvature and angles close to 180°. The curves are so tight that the two straight sides touch at the inner edge of the curve. For the models created, this is only a real issue for the 0.5 mm radius of curvature, and angles greater than 160°; in particular, the 0.5 mm radius of curvature is so small that the 180° model has both straight sides touching, and this means that data sets at those extremes are unreliable.

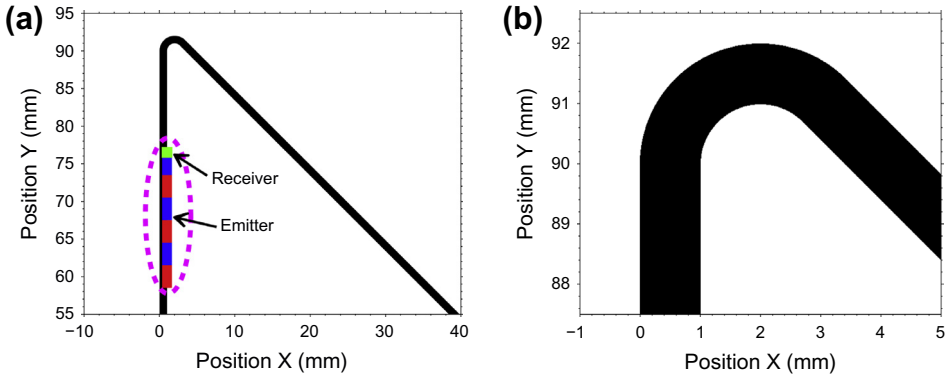

Fig. 3. An example curve, with a radius of curvature of 1.5 mm, and a bend of 135° (a). The green square is a receiver, and the red and blue regions (surrounded by a magenta dashed ellipse for visual clarity) are emitter elements, which combine to model a six element PPM SH-EMAT, of wavelength 6 mm. The curve itself (b) is as smooth as the model discretisation allows. (For interpretation of the references to colour in this figure legend, the reader is referred to the web version of this article.)

4.1. Simulation results

The time domain signal recorded for the 0° case was subtracted from each subsequent time domain data set that was captured. This process removed any unwanted signals, such as remaining oscillations due to the impulse cutting off abruptly, or reflections off the back edge. The process is perfect, in that it completely removes the unwanted signals without changing the signal of interest (the reflection from the curved section) at all. Such an ideal removal is possible in a simulation due to the conditions leading to the unwanted signals being absolutely identical in each case (the back edge and transducer positions are exactly the same), due to the complete absence of conventional noise, and due to the simulation being totally linear, such that the presence of a wave in no way changes the propagation of any other wave. The reflected signals were extracted from the simulation data using simple time-gating; no frequency filtering was necessary as simulated data has no conventional noise source. Fig. 4 compares a signal reflected from an edge (Fig. 4a), the case where there is no further medium into which to propagate, with the signals reflected from a 90° curve (Fig. 4b). Note that the amplitudes have been normalised, so that the peak-to-peak amplitude of the edge reflection is unity. There is a clear signal reflected in each case, although for the large radius curvature cases, the signal becomes very small.

The reflected signals were compared by taking the peak-to-peak amplitudes for each simulation, Fig. 5; values are relative to an edge reflection with a peak-to-peak amplitude of unity. Unlike what might be expected from initially considering the problem, except for the 0.5 mm radius of curvature case, the peak-to-peak amplitude of the reflected amplitude does not simply continue to increase. Although not shown here, the transmitted signal peak-to-peak amplitude shows similar behaviour to the reflected signal, but relative signal changes are very small compared to the absolute peak-to-peak amplitude of the transmitted signal itself.

There are spikes in the peak-to-peak amplitude at angles such as 45° (positive for the 2.0 mm case, negative for the 2.5 mm case) and 135° (another positive spike for the 2.0 mm case), and dips in the amplitude curve at angles such as 45° (for the 1.5 mm case) and 90° (for the 1.0 mm case). The exact reason for this is not currently known, but it is most likely due to the discrete and square nature of the simulation grid. At 90°, the second straight section forms a perfect horizontal line, and at 45° and 135° it forms a perfect diagonal, so that for each single change in vertical position there is a single change in horizontal position. At other angles, the second straight section must be approximated less precisely, and the variation of the quality of this approximation as the angle changes could lead to small errors at and close to these problem angles. This problem can be mitigated against by increasing the number of elements per wavelength in the simulation grid, but increasing this value beyond the current setting would lead to an unacceptable time to complete the simulation. The same issue occurred when checking the model for convergence at half the resolution, so it is unlikely that doubling the resolution again would resolve the issue completely, and hence seems of limited benefit.

4.2. Analytic approximation

A simple analytic model was created to consider the oscillation of the peak-to-peak amplitude of the reflected signal. This analytic model does not provide information on how much signal is reflected for a given radius, it simply assumes that a curve reflects a certain amount, and calculates what peak-to-peak amplitude is observed, if that amount is reflected.

The model starts with the approximation that each section of the curve reflects the same amount, and that the incoming signal is an infinite sine wave of angular frequency ω, and speed c. The overall signal received is then a combination of all the contributions from each part of the curve, and the signal, S, is given by an integration over the entire curve. Consider a total curve length of D, and a given position on the curve (relative to the start) is given by d, which is related to the current radius, r, and angle of curvature, θ, by $d = r\theta$. A wave must travel to that point on the curve, and back again, making a more useful variable $l = 2d = 2r\theta$, and $L = 2D$. Then, for the sinusoidal signal $\sin(\omega t)$, the resultant signal, S, is (where M is a normalising factor):

$$S = (1/M)\int_0^L \sin(\omega[t + l/c])\,dl \tag{5}$$

The time domain signal recorded for the 0° case was subtracted from each subsequent time domain data set that was captured.

The result is:

$$S = \{\sin(\omega t)\sin(\omega L/c) - \cos(\omega t)[\cos(\omega L/c) - 1]\}c/M\omega \tag{6}$$

To get the normalising factor, M, consider an infinite speed signal, such that every part of the reflection arrives simultaneously, and the parts of the signal combine perfectly. The integration is then just:

$$S_{inf} = (1/M)\int_0^L \sin(\omega t)\,dl = (L/M)\sin(\omega t) \tag{7}$$

The choice of normalising factor, based on this, is dependent on what S is intended to represent. The peak-to-peak amplitude is $2L/M$ (double the amplitude), and to make this unity, the normalising scale factor would be $M(r,\theta) = 2L = 4r\theta$. This normalising factor scales linearly with the angle and the radius of curvature, and

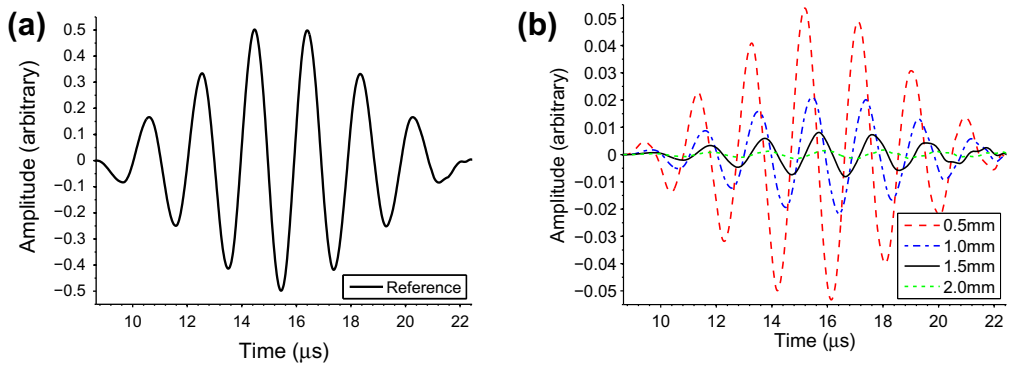

Fig. 4. FEM results comparing a wave reflected from an edge (a) and from a 90° curve (b). Although the amplitude is arbitrary in both cases, it is constant between the two plots, making it possible to directly compare the edge and curve reflected amplitudes. For reasons of clarity, the 2.5 mm and 3.0 mm radius of curvatures results are not shown in this figure.

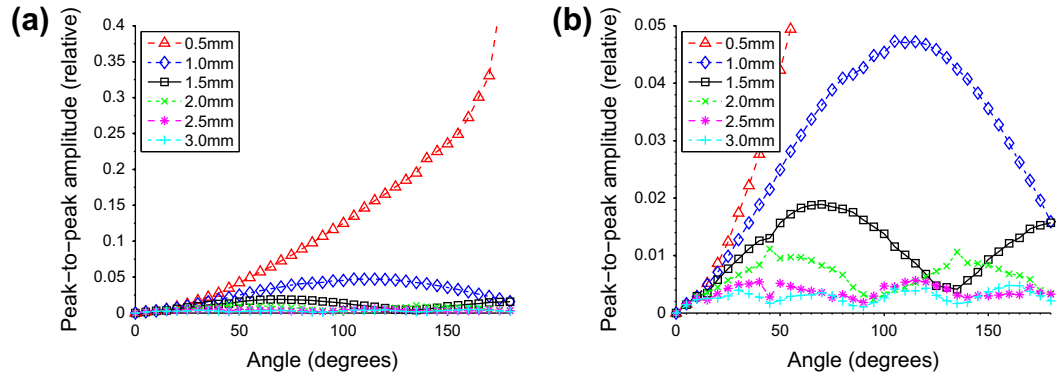

Fig. 5. The peak-to-peak amplitudes for each simulation, showing the overall levels (a) and providing a close-up of the 1 mm and higher radius of curvature cases (b).

hence what it leads S to represent, is the signal that would be observed just due to the interference between the different parts of the reflected signal. The normalising factor would remove any increase in the reflected signal due to the angle of the bend increasing, hence a 0° bend (the flat plate case) would reflect the same total energy as the 180° bend case. For comparison against experimental and FEM simulated data, it is more reasonable to make the normalising factor scale only with radius of curvature (as the amount of energy reflected should increase as the angle of the bend increases), and therefore, it is set to $M = 4\pi r$, the value of $2L$ for a bend at an angle of 180° (the maximum considered here). With this normalising factor, S represents the signal that would be observed due to the interference between the different parts of the reflected signal and the increase in the reflected signal as the angle of the bend increases, which is assumed in this model to be linear.

The peak-to-peak amplitude, of Eq. (6), can be extracted numerically from the result already obtained. However, it is a simple matter to differentiate $(dS(t)/dt)$ to find the maximum point in time for a given travel distance, which is when the following condition is met for the wave phase:

$$\omega t = \arctan\{\sin(\omega L/c)/[1-\cos(\omega L/c)]\} \tag{8}$$

Despite the relatively crude nature of the model, comparisons between this analytic approximation, Fig. 6, and the FEM simulation, Fig. 5b, show reasonable agreement in terms of the general shape, and the positions where maxima and minima appear. The model does not account for less energy being available for reflection at each subsequent point on the curve, but if the total energy reflected is a very small fraction of the total signal energy (the waves interact weakly with the bend), the error due to neglecting that factor is small. It is also assumed that once the wave energy is reflected, it returns from the direction it came without further interaction; again, if the waves interact weakly with the bend, the error due to neglecting that factor is small. Another issue not accounted for is the different radiuses of curvature on the inner and outer edges of the FEM modelled curve, which will be 0.5 mm larger on the outer edge, and 0.5 mm smaller on the inner edge, due to the FEM simulated thickness of 1 mm. However, the agreement with the FEM model does appear to provide some physical insight into the underlying effect, which was the objective of the analytic approximation. A similar physical cause is most likely true for the transmitted case (not shown here); variations in peak-to-peak amplitude are due to scattering events as the wave passes around the curved section.

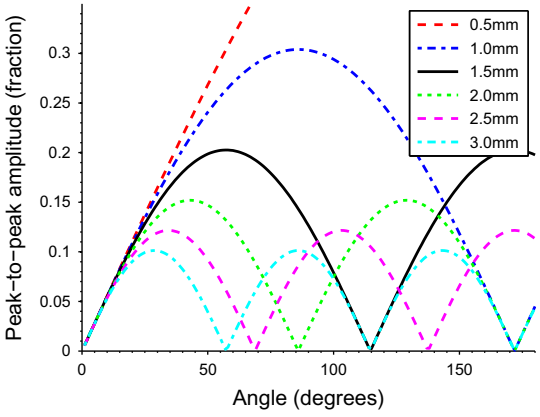

Fig. 6. The peak-to-peak amplitudes of the reflected signals from the analytic model. The amplitudes are not directly comparable to those in Fig. 5b, as the FEM simulation amplitudes are relative to a reflection from an edge, whereas the analytic model amplitudes are simply a fraction of the peak-to-peak amplitude that would be observed for a zero-delay 180° case.

5. Experimental measurements of SH guided wave propagation on curved sections

Tests were conducted using a 1 m square aluminium sheet, with a thickness of (0.83 ± 0.01) mm, measured at the edges using a micrometer, and a shear wave speed of 3060 m/s, measured in the same position that will be used for the propagation tests. In order to gather data for a range of angles, two 6 mm wavelength PPM SH-EMATs (a separate emitter and receiver), were fixed into position on a flat sample, a shallow bend was introduced, and a measurement of the reflected SH guided wave was taken. The EMATs were placed so that the emitter created a wave propagating directly towards the bend, and the polarisation of the wave was parallel to the line of the bend. The receiver was positioned directly in front of the emitter, and both were laterally in the centre of the plate, as shown in Fig. 7. The curve, which extended 1 m perpendicularly from one edge to the opposite edge, was 700 mm from the parallel edge on the side the emitter and receiver were placed. The centre of the emitter was 330 mm from the start of the curve, and the centre of the receiver was 280 mm from the start of the curve. Keeping the EMATs in the same position, the measurement was repeated as the angle of the bend was increased. Changing the radius of curvature experimentally is significantly more difficult than for a FEM simulation, and hence was kept constant at approximately (1.19 ± 0.2) mm for the inner radius. Based on the measurement of the inner radius and the thickness, the radius of curvature at a point halfway between the inner and outer surfaces would be (1.61 ± 0.2) mm, which is the equivalent radius of curvature used for the comparisons with the FEM simulations and the analytic approximation. Angles ranged from 0° (a completely straight section) to 135°, and as for the FEM simulations, the angle of curvature is measured as the deviation from the flat plate case,

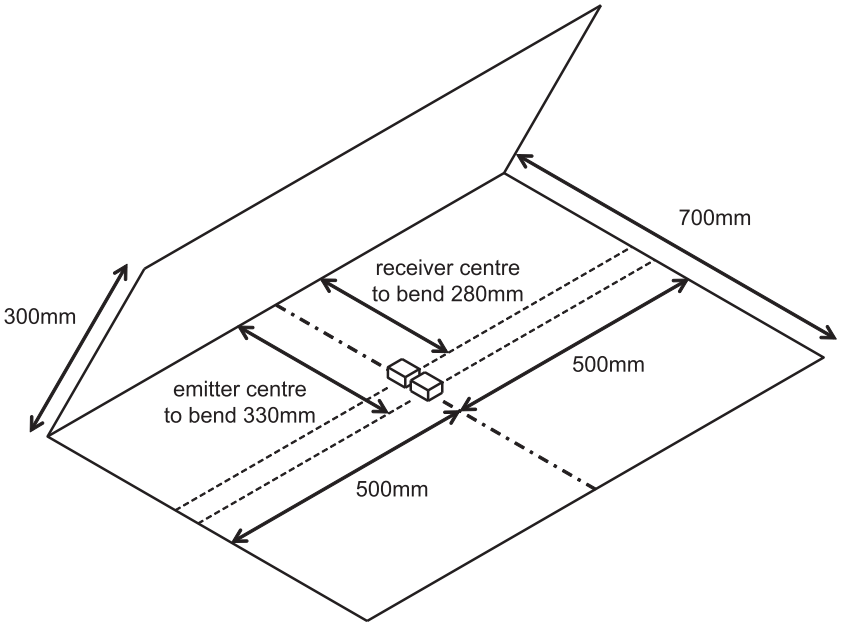

Fig. 7. Two 6 mm wavelength PPM SH-EMATs are placed on the (0.83 ± 0.01) mm thick aluminium sheet so that the SH guided wave propagates perpendicular to the line of the bend (directly towards it), with the emitter centre 330 mm from the bend, and the receiver centre 280 mm from the bend.

and represents the angle the plate has been bent by, rather than the internal angle of the curve.

During the experiments, it was important that the reflected wave did not suffer interference from other waves. The other waves include the direct wave from the emitter to the receiver, and waves reflected off the sample edges, for both SH0 and SH1 modes, as well as any Rayleigh–Lamb waves generated. The generation frequency that produced the largest peak-to-peak amplitude SH0 wave, received directly from the emitter, was 500 kHz, and a four cycle tone burst was used for the experiments, with a repetition rate of 10 Hz. The received signal was passed through an analogue band-pass filter with cut-off frequencies of 200 kHz and 2.5 MHz, recorded at a sampling frequency of 250 MHz, and then 256 captures were averaged to produce the final stored result. After digitisation, the received signals were band-pass filtered in the range 300–700 kHz, using a basic brick-wall filter, and the reflections extracted using simple time-gating. A comparison between the waves reflected from an edge and from the 90° curve can be seen in Fig. 8.

Fig. 9 shows that there is a reflected signal showing very good agreement between the experimental data and the analytic approximation, and a reasonable agreement between the FEM simulated data and the analytic approximation. The FEM simulation and analytic approximation were set up with the same parameters as the experiment for this comparison; thickness of 0.83 mm, a shear wave speed of 3060 m/s, and a radius of curvature at a point halfway between the inner and outer surfaces of 1.61 mm. The FEM simulation and analytic approximation data was taken at the same curve angles as measured in the experiment. The good agreement between the experiment and analytic model suggests that the analytic approximation is a reasonable representation of the actual reflection process from the curve. It also suggests that any deviation due to the cold working of the material (which neither the FEM simulation nor the analytic model account for) is not significant in this case. Although the FEM simulation data agrees reasonably with the analytic approximation, the reason why it agrees less well than the experiment is not currently known. It is also interesting that the FEM simulation predicts a peak-to-peak amplitude that is approximately 35% higher than was observed experimentally, but that could be due to the use of a point receiver in the FEM simulation, whereas the experiment had to use another PPM EMAT.

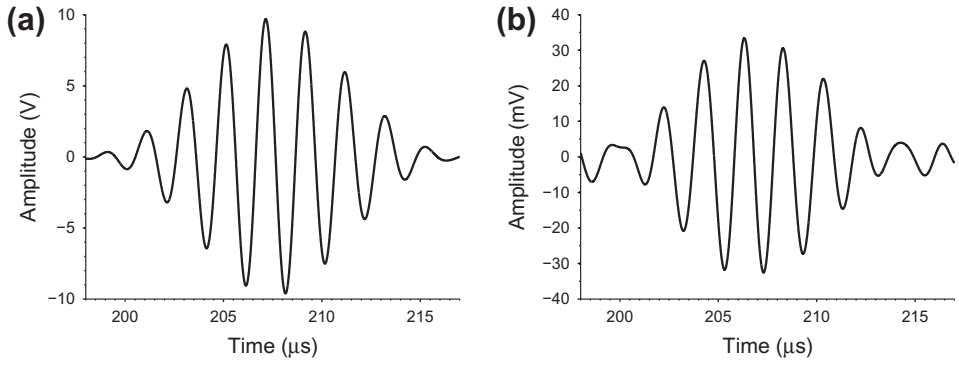

Fig. 8. The SH0 ultrasonic waves received after reflection from an edge (a) and from a 90° curve (b) with an approximate 1.61 mm radius of curvature. Although they can be compared to each other, they are not directly comparable to the FEM simulations.

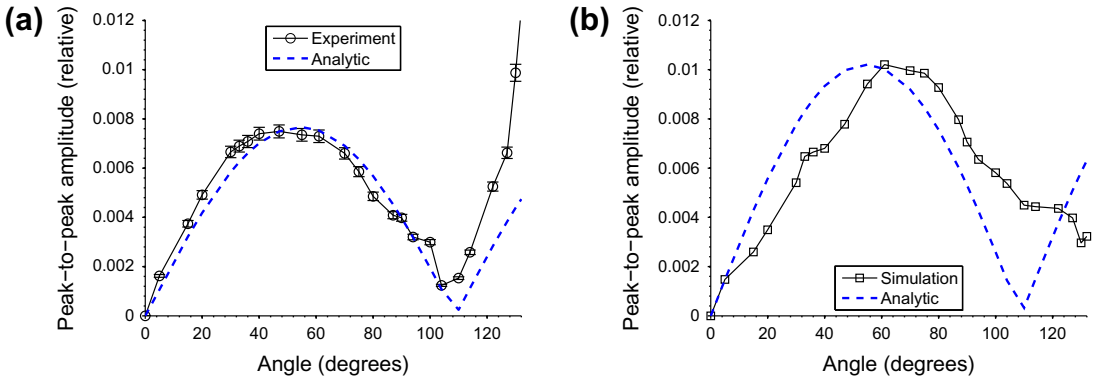

Fig. 9. A comparison (a) of the experimental data (solid black line, points marked with circles and error bars), and the analytic approximation (dashed blue line), alongside a comparison (b) of the FEM simulation data (solid black line, points marked with squares), and the analytic approximation (dashed blue line). The analytic approximation peak-to-peak amplitude has been scaled to match that of the experimental (a) or FEM simulated (b) data respectively, allowing for a better comparison of the form of the predicted response. (For interpretation of the references to colour in this figure legend, the reader is referred to the web version of this article.)

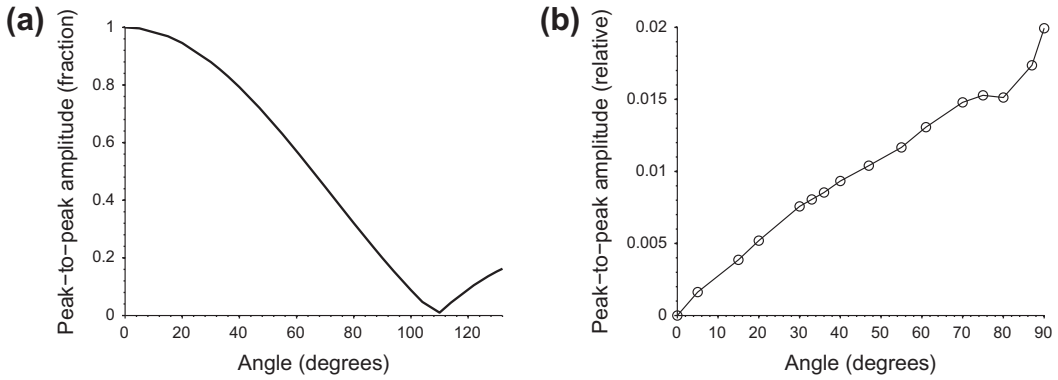

Fig. 10. Using a normalising factor $M(r,\theta) = 2L$, the analytic approximation to the reflected peak-to-peak amplitudes (a), can be used to scale the experimental data from Fig. 9a to compensate for the different parts of the reflection appearing at different times (b). In this case, the normalising factor means that the analytic approximation shows how the peak-to-peak amplitude changes just due to phase interference (a), whereas in Fig. 9a, the analytic approximation also factored in the increase in reflection due to a bend existing over a greater angle. The result of compensating for the phase interference shows that the increase in the reflected signal as the bend increases is approximately linear (b).

If the analytic approximation can be taken as a reasonable representation, then it can be used to assess what the total reflected signal would be if the waves combined perfectly (no destructive interference). To achieve this, the normalising factor is set to $M(r,\theta) = 2L = 4r\theta$, such that it scales with the angle of the bend, and this change is shown in Fig. 10a for the analytic approximation originally shown in Fig. 9. The analytic approximation now represents the change in peak-to-peak amplitude due only to the interference between the different reflected parts of the wave. The peak-to-peak amplitude that would be observed for the experimental case of a bend being increased from 0° to 90°, if all the waves combined coherently, rises approximately linearly from 0% to 2% of the peak-to-peak amplitude of an edge reflection, as shown in Fig. 10b, obtained simply by dividing the experimental data of Fig. 9a by the analytic approximation of 10a. This gives a measure of the total energy that is actually reflected, rather than what is observed. After traversing five 90° curves with a radius of curvature of 1.61 mm, the transmitted peak-to-peak amplitude would be expected to be 90% of its original value.

6. Conclusions

SH guided waves can easily propagate around curved sections of a sample with minimal reflection, and hence could potentially be used to detect defects over relatively long distances, despite the presence of bends and other obstructions. There is a clear relationship between the angle of the bend and the reflected signal, and the agreement between the experimental results and the analytic model suggest that the overall reflection observed is a linear superposition of the reflections from each segment of the curve. Consequently, sharp turns lead to a larger peak-to-peak amplitude due (in part) to greater phase coherence, but the total reflection is still very small. The slow dissipation of the SH guided waves is something that should be accounted for within other applications. More generally, it is likely that a similar relationship would be observed for other guided waves being reflected at a curved surface, but this has not been verified.

Acknowledgements

This work was supported by the Engineering and Physical Sciences Research Council (EPSRC), Grant EP/I03160X/1. The authors would also like to acknowledge the help provided by Lee Butcher in the Mechanical Workshop (University of Warwick, Department of Physics), with regards to bending the samples.

References

[1] K.F. Graff, Wave Motion in Elastic Solids, Dover Publications, New York, USA, 1975.
[2] J.L. Rose, Ultrasonic Waves in Solid Media, Cambridge University Press, Cambridge, UK, 1999.
[3] C.B. Scruby, L.E. Drain, Laser Ultrasonics: Techniques and Applications, Adam Hilger, Bristol, UK, 1990.

[4] J. Krautkramer, H. Krautkramer, Ultrasonic Testing of Materials, fourth ed., Springer-Verlag, Berlin, Germany, 1990.
[5] C.M. Fortunko, J.C. Moulder, Ultrasonic inspection of stainless steel butt welds using horizontally polarized shear waves, Ultrasonics 20 (1982) 113–117.
[6] J.A. Ogilvy, Ultrasonic beam profiles and beam propagation in an austenitic weld using a theoretical ray tracing model, Ultrasonics 24 (1986) 337–347.
[7] G. Hubschen, H.J. Salzburger, Inspection of dissimilar metal welds using horizontally polarized shear (SH-)waves and electromagnetic ultrasonic (EMUS-)probes, Int. J. Press. Vessels Piping 39 (1989) 331–344.
[8] K. Sawaragi, H.J. Salzburger, G. Hubschen, K. Enami, A. Kirihigashi, N. Tachibana, Improvement of SH-wave EMAT phased array inspection by new eight segment probes, Nucl. Eng. Des. 198 (2000) 153–163.
[9] H.J. Salzburger, G. Dobmann, H. Mohrbacher, Quality control of laser welds of tailored blanks using guided waves and EMATs, IEE Proc. – Sci. Measure. Technol. 148 (2001) 143–148.
[10] H.J. Salzburger, F. Niese, G. Dobmann, EMAT pipe inspection with guided waves, Weld. World 56 (2012) 35–43.
[11] Nurmalia, N. Nakamura, H. Ogi, M. Hirao, K. Nakahata, Mode conversion behavior of SH guided wave in a tapered plate, NDT & E Int. 45 (2012) 156–161.
[12] S. Dixon, P. Petcher, Y. Fan, D. Maisey, P. Nickolds, Ultrasonic metal sheet thickness measurement without prior wave speed calibration, J. Phys. D: Appl. Phys. 46 (2013) 445502.
[13] T. Hayashi, M. Murase, Mode extraction technique for guided waves in a pipe, Nondestruct. Test. Eval. 20 (2005) 63–75.
[14] T. Hayashi, M. Murase, Defect imaging with guided waves in a pipe, J. Acoust. Soc. Am. 117 (2005) 2134–2140.
[15] X. Zhao, J.L. Rose, Guided circumferential shear horizontal waves in an isotropic hollow cylinder, J. Acoust. Soc. Am. 115 (2004) 1912–1916.
[16] H.L. Grubin, Direct electromagnetic generation of compressional waves in metals in static magnetic fields, IEEE Trans. Son. Ultrason. 17 (1970) 227–229.
[17] K. Kawashima, Theory and numerical calculation of the acoustic field produced in metal by an electromagnetic ultrasonic transducer, J. Acoust. Soc. Am. 60 (1976) 1089–1099.
[18] R.B. Thompson, Ultrasonic Measurement Methods, Physical Acoustics, vol. XIX, Academic Press, London, UK, 1990, pp. 157–200.
[19] K. Kawashima, O.B. Wright, T. Hyoguchi, High frequency resonant electromagnetic generation and detection of ultrasonic waves, Jpn. J. Appl. Phys. Part 1 – Reg. Papers Short Notes Rev. Papers 33 (1994) 2837–2845.
[20] M. Hirao, H. Ogi, Electromagnetic acoustic resonance and materials characterization, Ultrasonics 35 (1997) 413–421.
[21] H. Ogi, Field dependence of coupling efficiency between electromagnetic field and ultrasonic bulk waves, J. Appl. Phys. 82 (1997) 3940–3949.
[22] S. Dixon, C. Edwards, S.B. Palmer, High accuracy non-contact ultrasonic thickness gauging of aluminium sheet using electromagnetic acoustic transducers, Ultrasonics 39 (2001) 445–453.
[23] M. Hirao, H. Ogi, EMATS for Science and Industry: Noncontacting Ultrasonic Measurements, Kluwer Academic Publishers, London, UK, 2003.
[24] C.F. Vasile, R.B. Thompson, Excitation of horizontally polarized shear elastic waves by electromagnetic transducers with periodic permanent magnets, J. Appl. Phys. 50 (1979) 2583–2588.
[25] M. Hirao, H. Ogi, An SH-wave EMAT technique for gas pipeline inspection, NDT & E Int. 32 (1999) 127–132.
[26] H. Ogi, E. Goda, M. Hirao, Increase of efficiency of magnetostriction SH-wave electromagnetic acoustic transducer by angled bias field: piezomagnetic theory and measurement, Jpn. J. Appl. Phys. Part 1 – Reg. Papers Short Notes Rev. Papers 42 (2003) 3020–3024.
[27] Y. Ohtsuka, M. Higashib, M. Nishikawa, Fundamental experiment for inspection of cooling pipes in operation by using ultrasonic technique, Fusion Eng. Des. 81 (2006) 1583–1587.